h/e Superconducting Quantum Interference through Trivial Edge States in InAs

Folkert K. de Vries,[1] Tom Timmerman,[1] Viacheslav P. Ostroukh,[2] Jasper van Veen,[1] Arjan J. A. Beukman,[1] Fanming Qu,[1] Michael Wimmer,[1] Binh-Minh Nguyen,[3] Andrey A. Kiselev,[3] Wei Yi,[3] Marko Sokolich,[3] Michael J. Manfra,[4] Charles M. Marcus,[5] and Leo P. Kouwenhoven[1,6,*]

[1]*QuTech and Kavli Institute of Nanoscience, Delft University of Technology, 2600 GA Delft, The Netherlands*
[2]*Instituut-Lorentz, Universiteit Leiden, P.O. Box 9506, 2300 RA Leiden, The Netherlands*
[3]*HRL Laboratories, 3011 Malibu Canyon Road, Malibu, California 90265, USA*
[4]*Department of Physics and Astronomy and Station Q Purdue, Purdue University, West Lafayette, Indiana 47907, USA*
[5]*Center for Quantum Devices and Station Q Copenhagen, Niels Bohr Institute, University of Copenhagen, Copenhagen, Denmark*
[6]*Microsoft Station Q Delft, 2600 GA Delft, The Netherlands*

(Received 12 September 2017; published 26 January 2018)

Josephson junctions defined in strong spin orbit semiconductors are highly interesting for the search for topological systems. However, next to topological edge states that emerge in a sufficient magnetic field, trivial edge states can also occur. We study the trivial edge states with superconducting quantum interference measurements on nontopological InAs Josephson junctions. We observe a SQUID pattern, an indication of superconducting edge transport. Also, a remarkable h/e SQUID signal is observed that, as we find, stems from crossed Andreev states.

DOI: 10.1103/PhysRevLett.120.047702

Topological systems are a hot topic in condensed matter physics [1]. This is largely motivated by the existence of states at the interface between two topologically distinct phases, for example helical edge states in a quantum spin Hall insulator (QSHI) [2,3]. Inducing superconductivity in these edge states would form a topological superconductor [1]. Superconducting edge transport has already been found in materials that are predicted to be a QSHI [4,5]. However, edge states can also have a nontopological origin. Trivial edge conduction is found in InAs alongside the chiral edge states in the QH regime [6] and recently in the proposed QSHI InAs/GaSb as well [7,8]. To be able to discriminate between topological and trivial states, it is crucial to study transport through trivial edges also and clarify differences and similarities between them. In this work we study the superconducting transport through trivial edge states in nontopological InAs Josephson junctions using superconducting quantum interference (SQI) measurements. We find a supercurrent carried by these edge states and an intriguing h/e periodic signal in a superconducting quantum interference device (SQUID) geometry.

Trivial edge states arise when the Fermi level resides in the band gap in the bulk, while being pinned in the conduction band at the surface. Then, band bending leads to electron accumulation at that surface as schematically drawn in Fig. 1(a). The Fermi level pinning can have several origins: truncating the Bloch functions in space [9,10], a work function difference [11], the built-in electric field in a heterostack [12], and the surface termination [13]. In our 2D InAs Josephson junctions the accumulation surface is located at the edge of the mesa that is defined by wet etching. The quantum well is MBE grown on a GaSb substrate serving as a global bottom gate [14]. The superconducting electrodes are made of sputtered NbTiN with a spacing of 500 nm and a width of 4 μm. NbTiN has a bulk superconducting gap of 2 meV and a critical temperature of 13 K. A SiN_x dielectric separates the top gate from the heterostructure. Electrical quasifour terminal measurements [see Fig. 1(b)] are performed in a dilution refrigerator with an electron temperature of 60 mK unless stated otherwise.

The electron density in the InAs quantum well is altered by using the electrostatic gates, V_{tg} and V_{bg}, located above and below the 2DEG. Decreasing the density subsequently increases the normal state resistance R_n and reduces the switching current I_s as shown in Fig. 2(a). A full resistance map as a function of the top and bottom gate is shown in the Supplemental Material [14]. The Josephson junction is first characterized at $V_{\mathrm{tg}} = 0$ V and $V_{\mathrm{bg}} = -1.65$ V, where the largest switching current is observed. From the IV trace in Fig. 2(a) we estimate an induced superconducting gap of 0.4 meV and, using the corrected Octavio-Blonder-Tinkham-Klapwijk model [20], a transmission of $T = 0.73$. The junction is quasiballistic because the mean free path of 2.8 μm (extracted from a Hall bar device on the same wafer [14]) is larger than its length L of 500 nm. The large superconducting gap and high transmission value indicate a high quality InAs Josephson junction.

SQI measurements have successfully been used before to gather information on the supercurrent density profile in Josephson junctions [4,5,21]. This is typically done, using the Dynes-Fulton approach [22], which connects the

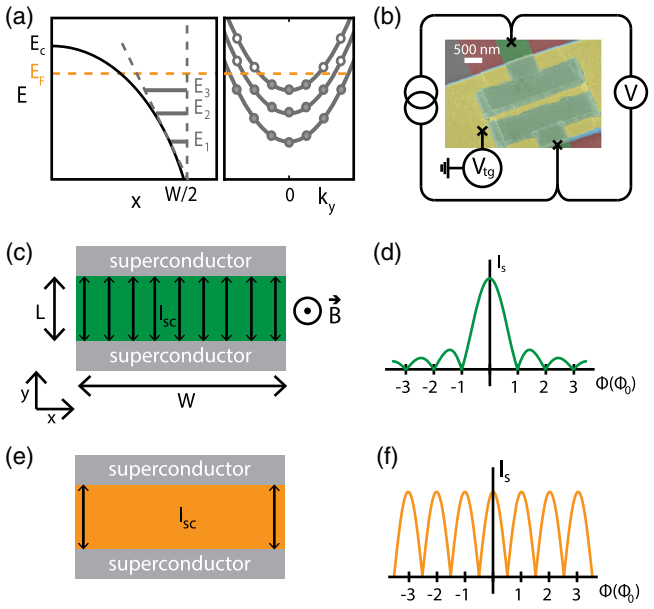

FIG. 1. (a) Sketch of the conduction band minimum around the edge of a 2DEG with Fermi level pinning at $W/2$. The band bending leads to a roughly triangular quantum well in the vicinity of the edge; therefore, one-dimensional subbands form, of which three are drawn, as an example. The orange dashed line indicates the Fermi level corresponding to the current distribution in (e). (b) False colored SEM image of the device with dimensions $W = 4\ \mu$m and $L = 500$ nm, where the quasifour terminal measurement setup is added. Red is the mesa, green the NbTiN contacts, blue SiN_x dielectric, and yellow the gold top gate. (c) Schematic representation of a Josephson junction of width W and length L. A homogeneously distributed supercurrent I_{sc} is running through the whole junction, resulting in (d) a Fraunhofer SQI pattern. (e) If the supercurrent only flows along the edges of the sample, (f) a SQUID pattern is observed.

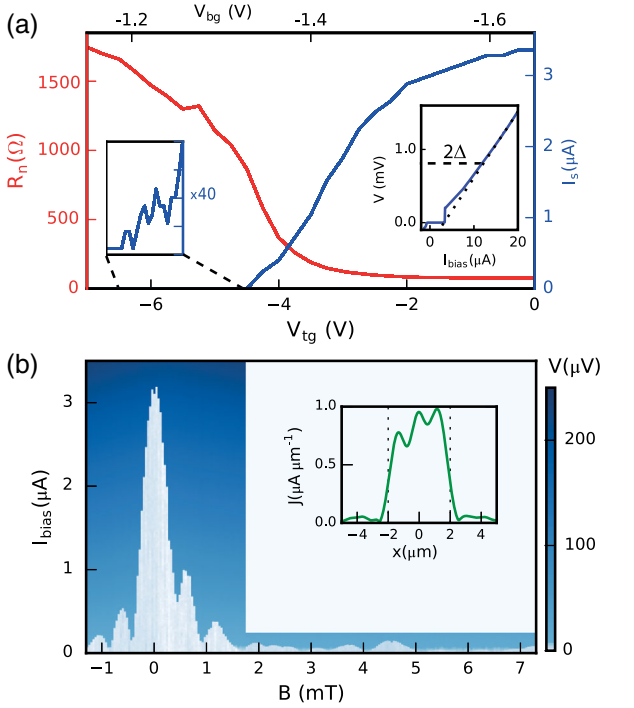

FIG. 2. (a) Normal state resistance R_n and switching current I_s at the respective top gate V_{tg} and bottom gate V_{bg} voltages. The left inset depicts a separate measurement at the indicated gate voltages, where a smaller current bias step size is used for higher resolution. The right inset shows an IV trace at $V_{tg} = 0$ V and $V_{bg} = -1.65$ V, where two dashed lines are added for extraction of the induced superconducting gap Δ and the excess current. (b) The measured voltage as function of the applied current I_{bias} and perpendicular magnetic field B at $V_{tg} = 0$ V and $V_{bg} = -1.65$ V. The inset depicts the calculated supercurrent density along the width of the device that is indicated by the dotted lines.

critical current dependency on magnetic field $I_c(B)$ and the zero-field supercurrent density profile $j(x)$ with a Fourier transform. It was originally developed for tunnel junctions, but can also be applied to transparent junctions under several assumptions. First, we should have a sinusoidal current-phase dependency, which is in accordance with the transmission value and temperature in our experiment [23]. Second, the Andreev levels, that carry a supercurrent in the junction, may only weakly deviate from the longitudinal propagation. Our junction satisfies this constraint since the superconducting coherence length $\zeta = \hbar v_F/\Delta \approx 1.3\ \mu\text{m} > L$ [14,24]. If both assumptions hold, we expect a Fraunhofer SQI pattern in the case of homogeneous current distribution [Figs. 1(c) and 1(d)] and a SQUID pattern in the case of current flowing along the edges [Fig. 1(e) and 1(f)].

A SQI measurement at the largest switching current reveals a Fraunhofer-like pattern as shown in Fig. 2(b). The central lobe is twice as wide as the side lobes and the amplitude decreases as expected. The slight asymmetry in the amplitudes we attribute to breaking of the mirror symmetry of the sample in the direction along the current [25]. The effective length of the junction [$\lambda = \delta B_{\text{lobe}}/(\Phi_0 W)$] of 1.2 μm is extracted from the periodicity of the SQI pattern. Flux focusing due to the Meissner effect causes it to be larger than the junction length ($\lambda > L$) [26]. The extracted current density profile, plotted in Fig. 2(b), is close to uniform. The supercurrent is thus dominated by bulk transport as expected at these gate voltages.

The interference pattern in Fig. 2(b) deviates from the expected pattern after the second lobe. Recently a similar distorted Fraunhofer tail was observed and discussed in graphene [27]. The perpendicular magnetic field exerts a Lorentz force on the electron and holes suppressing the formation of Andreev bound states. The suppression becomes relevant at a magnetic field scale of Δ/eLv_F, equal to 1 mT in our case, roughly agreeing with the observation. The analysis only holds for the bulk of the junction, since the scattering at the edges reduces the difference in the electron and hole motion in a magnetic field.

Next we study the SQI pattern as the Fermi level is decreased by tuning the top gate to more negative values.

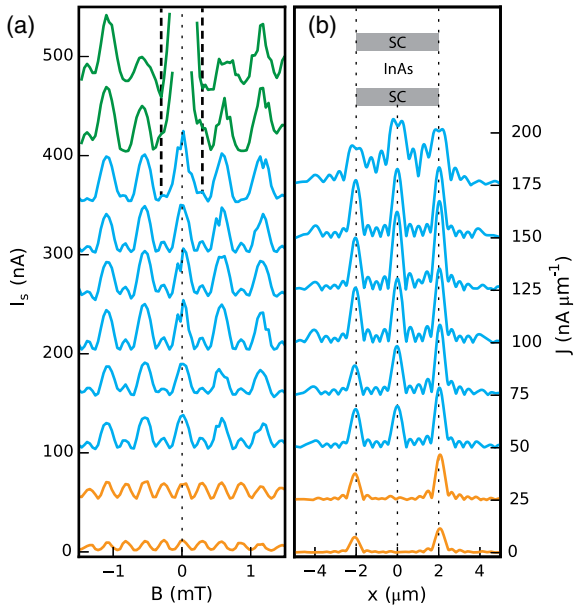

FIG. 3. (a) The switching current plotted as a function of perpendicular magnetic field and (b) the corresponding current density along the width of the device (see inset), assuming the validity of the Dynes-Fulton approach. The gate values used are from bottom to top: V_{tg} − 5.4 V to −3.6 V (0.2 V step) and V_{bg} − 1.270 V to −1.396 V (0.014 V step). The green, blue, and orange traces are Fraunhofer, even-odd, and SQUID patterns, respectively. Since the current is only swept up to 100 nA, the green traces are not suitable for extracting a supercurrent density profile. The traces are offset by 50 nA in (a) and 25 nA/μm in (b).

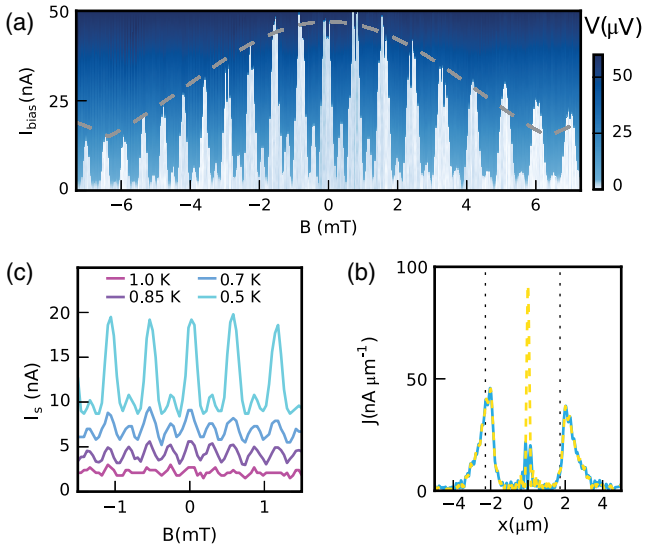

FIG. 4. (a) Measured voltage as a function of I_{bias} and magnetic field B at $V_{tg} = -5$ V and $V_{bg} = -1.29$ V. (b) Switching current versus the magnetic field for different temperatures at the same gate voltages as (a). The traces are offset by 5 nA for clarity. (c) Current density profile, calculated from the SQI pattern of (a) (see also Ref. [14]). The blue trace uses Eq. (1), thus correcting the vertical offset in the SQI pattern. The yellow dashed trace is extracted without this correction.

The upper two (green) traces in Fig. 3(a) have a wide central lobe, stemming from a Fraunhofer pattern. The side lobes, however, do not decrease in amplitude, as expected, but seem to be constant, as for an SQUID pattern. We conclude that we are in the transition regime from bulk to edge transport. The effective length is $\lambda = 1.7$ μm, different from before, which we believe is due to different vortex pinning because of the larger magnetic field range of the measurement [14]. In the third (first blue) trace we observe that the first nodes turn into peaks, which is highlighted by the dashed lines. Therefore, the transition to a SQUID pattern is completed. Curiously, the amplitude and width of the peaks are alternating in the blue traces in Fig. 3(a). The even-odd pattern is composed of an h/e and $h/2e$ periodic signal. An even-odd pattern was observed before in Pribiag *et al.* [5]. In comparison, in this work the amplitude difference in the lobes is much larger and the pattern is visible over a large gate range. The calculated supercurrent density profiles in Fig. 3(b) have a central peak that is physically unlikely considering the device geometry. The cause of this intriguing interference pattern will be discussed in more detail later. Reducing V_{tg} further, we find a clear $h/2e$ periodic SQUID interference pattern in the bottom two (orange) traces. This is a strong indication of edge conduction in our device, confirmed by the edge transport only in the extracted supercurrent density profiles in Fig. 3(b). The transition from bulk to edge transport as a function of gate voltage is measured in several other Josephson junctions [14]. Since we observe a supercurrent through the trivial edge states of an InAs quantum well, we conclude that a clear demonstration of superconducting edges alone does not prove induced superconductivity in topological edge states.

We now return to the remarkable h/e SQUID signal to investigate its origin. Figure 4(a) shows a more detailed measurement in this gate regime, the even-odd pattern is observed over more than 25 oscillations. The envelope of the peaks is attributed to the finite width of the edge channels. The effect is suppressed by raising the temperature [see Fig. 4(b)], for $T > 850$ mK a regular $h/2e$ SQUID pattern remains. The origin cannot lie in effects that occur beyond a certain critical magnetic field, like $0-\pi$ transitions [28], edge effects [29,30], and a topological state, because we observe the even-odd pattern around zero magnetic field as well. An effect that does not rely on magnetic field and is strongly temperature dependent is crossed Andreev reflection [31].

The lowest order crossed Andreev reflection (up to electron-hole symmetry) is schematically depicted in Fig. 5(a). An electron travels along one edge, whereafter a hole is retroreflected over the other edge. This process alone is independent of the flux through the junction, but still adds to the critical current [32]. Higher order processes that include an electron that encircles the junction

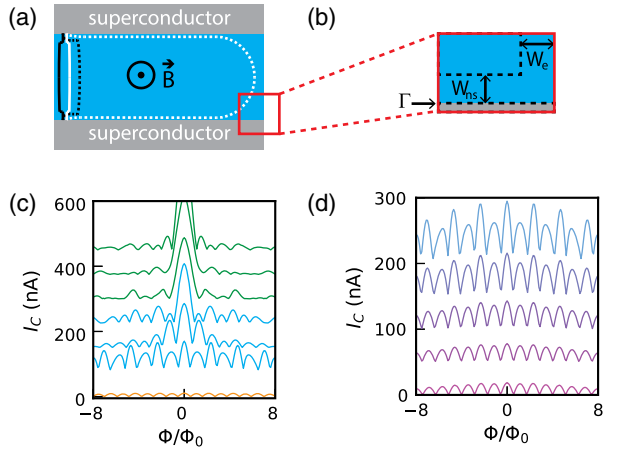

FIG. 5. (a) Schematic representation of two crossed Andreev processes. The black and white lines indicate electron and hole trajectories or vice versa. The solid lines represent a single edge Andreev state and the dotted lines a crossed Andreev state. (b) Detailed sketch of one corner of the junction in our tight binding mode indicating the widths W_{ns} and W_e, and tunnel barrier Γ. (c) Calculated SQI patterns at overall chemical potential ranging from −0.06 eV to 0.18 eV (0.04 eV step) at 0.46 K and (d) at temperatures 0.4 K, 0.9 K, 1.4 K, 1.9 K, 2.3 K at a chemical potential of −0.2 eV. Traces are offset by 10 nA for clarity. In (c) the color represents the type of interference pattern, green for Fraunhofer, blue for even-odd, and orange for SQUID, respectively.

completely pick up an h/e phase when a flux quantum threads through the junction; hence, the supercurrent becomes h/e periodic [33,34]. Additionally, interference processes between crossed Andreev and single edge Andreev states could lead to a h/e contribution [35]. It is important to note that the critical current is h/e periodic in flux trough the sample, but still 2π periodic in the superconducting phase difference.

Forming crossed Andreev states in the junction is only possible if the particles can flow along the contacts. Electrostatic simulations indeed show a large electron density close to the contacts at gate voltages where the bulk is already depleted [14], because of local screening of the top gate. Nevertheless the needed coherence length for a crossed Andreev reflection is on the order of 10 μm, where the estimated superconducting coherence length (from bulk values) is 1.3 μm. The difference between these values remains an open question.

The phenomenological model proposed by Baxevanis *et al.* considers both single edge and crossed Andreev states [32]. In our device we expect the lowest order crossed Andreev states to contribute most because of the short coherence length. Combining their flux insensitive contribution to the critical current and the usual $h/2e$ periodic contribution from single edge Andreev bound states, the model predicts an even-odd or h/e SQUID pattern:

$$I_c(\Phi) = I_0|\cos(\pi\Phi/\Phi_0) + f|, \tag{1}$$

where I_0 is the critical current at zero magnetic field and Φ is the applied flux. Constant f can be arbitrarily large, it depends on the ratio Γ between the probability to Andreev reflect on a node versus the probability to scatter to another edge and is exponentially suppressed by the width of the sample:

$$f \sim \Gamma^{-1}\frac{k_B T}{\Delta} e^{-2\pi(k_B T/\Delta)(W/\zeta)}. \tag{2}$$

The predicted pattern is thus the absolute value of a vertically offset cosine function. That is exactly the pattern we measured in Figs. 3(a) and 4(a) as both the amplitude and width of the lobes alternate (see also Ref. [14]). From the data we estimate $f = 0.3$ and, using the other known parameters, find $\Gamma \sim 10^{-1}$. Taking the Fourier transform in the Dynes-Fulton analysis, offset f leads to a nonphysical current density around zero, like we observe in the current density profiles in Fig. 3(b) and the yellow dashed line in Fig. 4(c). Moreover, the Dynes-Fulton approach is not valid here since crossed Andreev reflection does not meet the second assumption of having straight trajectories only. We can compensate the crossed Andreev contribution by subtracting the constant offset of $fI_0 = 11$ nA. This results in a current distribution with mainly current along the edges, as plotted in the blue trace of Fig. 4(c). We did not take into account that I_0 is actually not constant due to the Fraunhofer envelope of the SQI pattern, so the current density in the center of the junction is not entirely eliminated.

Even though the SQI pattern from the phenomenological model is in qualitative agreement with our data, we also present a tight binding model of system in order to connect it directly to experimentally accessible parameters. In the microscopic model we include the superconducting gap as measured, the width of the paths along the contacts W_{ns} of 20 nm [extracted from the Fraunhofer envelope in Fig. 4(a)], and Fermi level pinning on the edges leading to edge current in the region W_e. It is crucial to also take into account a tunnel barrier Γ at the contacts that has a magnitude consistent with the measured transmission value. This barrier enhances normal reflection and therefore elongates the length electrons and holes travel before Andreev reflecting [14]. Incorporating these experimental values we find an h/e SQUID pattern. Emulating the experimental gating effect by changing the overall chemical potential results in a crossover from even-odd to Fraunhofer [Fig. 5(c)], consistent with the measurement in Fig. 3. As a check, W_{ns} is reduced in steps to zero, which results in a SQUID pattern [14]. Additionally, in Fig. 5(d) we observe that increasing the temperature indeed smears out the even-odd pattern and leaves us with a regular SQUID pattern, similar to the experimental data in Fig. 4(b). Summarizing, both the phenomenological model and the microscopic model support our hypothesis of the h/e SQUID originating from crossed Andreev states.

We have experimentally shown that trivial edge states can support highly coherent superconducting transport that also becomes visible in an h/e periodic SQI pattern. Both effects have been considered as possible signatures for inducing superconductivity in topological edge states before [4,5]. Therefore, we conclude that superconducting edge transport and an h/e SQUID pattern only, cannot distinguish between topological and trivial edge states, nor can it be considered a definite proof for a topological phase.

We thank Daniel Loss for fruitful discussions and Carlo Beenakker and Michiel de Moor for useful comments on the Letter. This work has been supported by funding from the Netherlands Organisation for Scientific Research (NWO), Microsoft Corporation Station Q, the Danish National Research Foundation, and an ERC Synergy Grant.

*l.p.kouwenhoven@tudelft.nl

[1] M. Z. Hasan and C. L. Kane, Rev. Mod. Phys. **82**, 3045 (2010).
[2] C. L. Kane and E. J. Mele, Phys. Rev. Lett. **95**, 226801 (2005).
[3] M. König, S. Wiedmann, C. Brüne, A. Roth, H. Buhmann, L. W. Molenkamp, X.-L. Qi, and S.-C. Zhang, Science **318**, 766 (2007).
[4] S. Hart, H. Ren, T. Wagner, P. Leubner, M. Muhlbauer, C. Brune, H. Buhmann, L. W. Molenkamp, and A. Yacoby, Nat. Phys. **10**, 638 (2014).
[5] V. S. Pribiag, A. J. A. Beukman, F. Qu, M. C. Cassidy, C. Charpentier, W. Wegscheider, and L. P. Kouwenhoven, Nat. Nanotechnol. **10**, 593 (2015).
[6] B. van Wees, G. Meijer, J. Kuipers, T. Klapwijk, W. van de Graaf, and G. Borghs, Phys. Rev. B **51**, 7973 (1995).
[7] B.-M. Nguyen, A. A. Kiselev, R. Noah, W. Yi, F. Qu, A. J. A. Beukman, F. K. de Vries, J. van Veen, S. Nadj-Perge, L. P. Kouwenhoven, M. Kjaergaard, H. J. Suominen, F. Nichele, C. M. Marcus, M. J. Manfra, and M. Sokolich, Phys. Rev. Lett. **117**, 077701 (2016).
[8] F. Nichele, H. J. Suominen, M. Kjaergaard, C. M. Marcus, E. Sajadi, J. A. Folk, F. Qu, A. J. A. Beukman, F. K. de Vries, J. van Veen, S. Nadj-Perge, L. P. Kouwenhoven, B.-M. Nguyen, A. A. Kiselev, W. Yi, M. Sokolich, M. J. Manfra, E. M. Spanton, and K. A. Moler, New J. Phys. **18**, 083005 (2016).
[9] I. Tamm, Phys. Z. Soviet Union **1**, 733 (1932).
[10] W. Shockley, Phys. Rev. **56**, 317 (1939).
[11] J. Bardeen, Phys. Rev. **71**, 717 (1947).
[12] A. Furukawa, Appl. Phys. Lett. **62**, 3150 (1993).
[13] L. O. Olsson, C. B. M. Andersson, M. C. Håkansson, J. Kanski, L. Ilver, and U. O. Karlsson, Phys. Rev. Lett. **76**, 3626 (1996).
[14] See Supplemental Material at http://link.aps.org/supplemental/10.1103/PhysRevLett.120.047702 for additional data and details on the tight binding model, which includes Refs. [15–19].
[15] F. Qu, A. J. A. Beukman, S. Nadj-Perge, M. Wimmer, B.-M. Nguyen, W. Yi, J. Thorp, M. Sokolich, A. A. Kiselev, M. J. Manfra, C. M. Marcus, and L. P. Kouwenhoven, Phys. Rev. Lett. **115**, 036803 (2015).
[16] X. Mu, G. Sullivan, and R.-R. Du, Appl. Phys. Lett. **108**, 012101 (2016).
[17] G. Stan, S. B. Field, and J. M. Martinis, Phys. Rev. Lett. **92**, 097003 (2004).
[18] A. Furusaki, Physica (Amsterdam) **203B**, 214 (1994).
[19] C. W. Groth, M. Wimmer, A. R. Akhmerov, and X. Waintal, New J. Phys. **16**, 063065 (2014).
[20] K. Flensberg, J. B. Hansen, and M. Octavio, Phys. Rev. B **38**, 8707 (1988).
[21] M. T. Allen, O. Shtanko, I. C. Fulga, A. R. Akhmerov, K. Watanabe, T. Taniguchi, P. Jarillo-Herrero, L. S. Levitov, and A. Yacoby, Nat. Phys. **12**, 128 (2016).
[22] R. C. Dynes and T. A. Fulton, Phys. Rev. B **3**, 3015 (1971).
[23] W. Haberkorn, H. Knauer, and J. Richter, Phys. Status Solidi A **47**, K161 (1978).
[24] H.-Y. Hui, A. M. Lobos, J. D. Sau, and S. Das Sarma, Phys. Rev. B **90**, 224517 (2014).
[25] A. Rasmussen, J. Danon, H. Suominen, F. Nichele, M. Kjaergaard, and K. Flensberg, Phys. Rev. B **93**, 155406 (2016).
[26] H. J. Suominen, J. Danon, M. Kjaergaard, K. Flensberg, J. Shabani, C. J. Palmstrøm, F. Nichele, and C. M. Marcus, Phys. Rev. B **95**, 035307 (2017).
[27] M. Ben Shalom, M. J. Zhu, V. I. Fal'ko, A. Mishchenko, A. V. Kretinin, K. S. Novoselov, C. R. Woods, K. Watanabe, T. Taniguchi, A. K. Geim, and J. R. Prance, Nat. Phys. **12**, 318 (2016).
[28] T. Yokoyama, M. Eto, and Y. V. Nazarov, J. Phys. Soc. Jpn. **82**, 054703 (2013).
[29] J. P. Heida, B. J. van Wees, T. M. Klapwijk, and G. Borghs, Phys. Rev. B **57**, R5618 (1998).
[30] H. Meier, V. I. Fal'ko, and L. I. Glazman, Phys. Rev. B **93**, 184506 (2016).
[31] S. Russo, M. Kroug, T. M. Klapwijk, and A. F. Morpurgo, Phys. Rev. Lett. **95**, 027002 (2005).
[32] B. Baxevanis, V. P. Ostroukh, and C. W. J. Beenakker, Phys. Rev. B **91**, 041409 (2015).
[33] J. A. M. van Ostaay, A. R. Akhmerov, and C. W. J. Beenakker, Phys. Rev. B **83**, 195441 (2011).
[34] J. Liu, H. Liu, J. Song, Q.-F. Sun, and X. C. Xie, Phys. Rev. B **96**, 045401 (2017).
[35] P. Recher, E. V. Sukhorukov, and D. Loss, Phys. Rev. B **63**, 165314 (2001).